# High-Quality Ultralong Sb 2 Se 3 and Sb 2 S 3 Nanoribbons on a Large Scale via a Simple Chemical Route

**ARTICLE** *in* THE JOURNAL OF PHYSICAL CHEMISTRY B · AUGUST 2006

Impact Factor: 3.3 · DOI: 10.1021/jp061599d · Source: PubMed



**4 AUTHORS**, INCLUDING:

Y. Yu
Technical Institute of Physics and Chemistry
**34** PUBLICATIONS **1,178** CITATIONS
SEE PROFILE

Qing Chen
Peking University
**173** PUBLICATIONS **6,004** CITATIONS
SEE PROFILE

Lian-Mao Peng
Peking University
**396** PUBLICATIONS **9,731** CITATIONS
SEE PROFILE

# High-Quality Ultralong $Sb_2Se_3$ and $Sb_2S_3$ Nanoribbons on a Large Scale via a Simple Chemical Route

**Y. Yu,[†] R. H. Wang,[†] Q. Chen,[‡] and L.-M. Peng*[,‡]**

*Beijing Laboratory of Electron Microscopy, Institute of Physics, Chinese Academy of Science, Beijing 100080, China, and Key Laboratory on the Physics and Chemistry of Nanodevices and Department of Electronics, Peking University, Beijing 100871, China*

*Received: March 15, 2006; In Final Form: May 9, 2006*

Large-scale ultralong single-crystalline $Sb_2Se_3$ and $Sb_2S_3$ nanoribbons were prepared respectively by reacting $SbCl_3$ with selenium and sulfur powders in glycol solution. Both $Sb_2Se_3$ and $Sb_2S_3$ nanoribbons are usually hundreds of microns in length, and the structures of the nanoribbons are determined to be of the orthorhombic phases. The $Sb_2Se_3$ nanoribbons are typically 100−300 nm in width and 20−60 nm in thickness and grow along the $[1\bar{1}2]$ direction. $Sb_2S_3$ nanoribbons are wider than $Sb_2Se_3$ nanoribbons; $Sb_2S_3$ nanoribbons are about 200−500 nm in width and grow along the [001] direction. The growth mechanism of the nanoribbons is investigated based on high-resolution transmission electron microscopy (HRTEM) observations. Optical absorption experiment reveals that $Sb_2Se_3$ and $Sb_2S_3$ nanoribbons are two semiconductors with bandwidth $E_g \approx 1.15$ eV and $E_g \approx 1.56$ eV, respectively.

## 1. Introduction

In recent years one-dimensional semiconductor nanomaterials, including nanotubes, nanowires, and nanoribbons, have attracted considerable interest for scientific research because of their remarkable electronic, magnetic, optical, catalytic, and mechanical properties, which are different from those of bulk materials. These nanomaterials may eventually lead to applications in nanodevices.[1−3] Among these semiconductors, the main-group metal chalocogenides such as $V_2VI_3$ (V = As, Sb, Bi; VI = S, Se, Te) group compounds have applications in television cameras with photoconducting targets, in thermoelectric devices, in optoelectronic devices, and in IR spectroscopy.[4−6] $Sb_2Se_3$ and $Sb_2S_3$ are two direct band gap semiconductors that crystallize in the orthorhombic system (*pbnm* space group) and are isostructural with $Bi_2S_3$.[7,8] $Sb_2Se_3$ and $Sb_2S_3$ have many good and useful properties for application. Rosi and co-workers found the Peltier effect in $Sb_2Se_3$ and utilized this effect for cooling.[9] Platakis et al. reported threshold and memory switching phenomena on the materials of $Sb_2Se_3$.[10] $Sb_2Se_3$ also exhibits excellent photovoltaic and thermoelectric properties.[11,12] $Sb_2S_3$ is an important semiconductor with high photosensitivity and thermoelectric power,[13] and is regard as a prospective material for solar energy due to its good photoconductivity.[14] It has also been used in thermoelectric cooling technology, and in photoelectronics in the IR region.[5,15] Owing to these good and useful properties, $Sb_2Se_3$ and $Sb_2S_3$ have been attracting great research attention. $Sb_2Se_3$ and $Sb_2S_3$ thin films[16−19] and one-dimensional materials including nanorods[20−23] and microtubes[24,25] have been synthesized by various methods. The newly distinct one-dimensional nanostructures with ribbonlike or beltlike morphologies, which are very promising for sensors due to the fact that the surface to volume ratio (S/V) is very high, have been successfully prepared for semiconducting metal oxides by evaporating the desired metal oxide powders at a high temperature.[26−28] A solution-phase approach (hydrothermal reaction) for preparing nanoribbons, which may provide a more promising method for nanoribbons than conventional methods in terms of cost and potential for large-scale production, has seldom been reported.[29,30] To the best of our knowledge, only two papers on $Sb_2Se_3$ and $Sb_2S_3$ nanoribbons have been published. One is about $Sb_2Se_3$ nanoribbons that were reported by Qian and co-workers.[30] These authors synthesized $Sb_2Se_3$ nanoribbons by reacting $SbCl_3$ and $Na_2SeSO_3$ with polymer assistance. The as-synthesized nanoribbons are about 30 $\mu$m in length, and their morphologies are related to the amount of the polymer. The other paper is about $Sb_2S_3$ nanoribbons reported in our previous paper.[31] We obtained $Sb_2S_3$ nanoribbons by directly reacting $SbCl_3$ and $Na_2S_2O_3$. The $Sb_2S_3$ nanoribbons grew from the decomposition of an amorphous compound of $Sb_xS_yO_z$. Herein, we report a simple hydrothermal method for synthesizing high-purity single-crystal $Sb_2Se_3$ and $Sb_2S_3$ nanoribbons with lengths of up to hundreds of microns by reacting $SbCl_3$ and Se and S powders in glycol solution with the assistance of $NaBH_4$. The $Sb_2Se_3$ nanoribbons and $Sb_2S_3$ nanoribbons grew from $Sb_2Se_3$ and $Sb_2S_3$ nanoparticles, respectively, which is distinct from our previous work on $Sb_2S_3$ nanoribbons. The structure, growth mechanism, and optical absorption at room temperature of the nanoribbons are investigated.

## 2. Experimental Section

All chemical reagents used in this experiment were of analytical grade. In a typical experimental for $Sb_2Se_3$ nanoribbons, 0.25 g of $SbCl_3$ was first added into 30 mL of distilled water; after stirring for 10 min, 30 mL of glycol was introduced and stirred continuously for 10 min. The mixed solution together with 0.2 g of selenium powder and 0.3 g of $NaBH_4$ was then transferred into a Teflon-lined stainless steel autoclave (80 mL capacity), sealed, and maintained at 180 °C for 3 days. After the reaction, the resulting black solid product was filtered, and

* To whom correspondence should be addressed. E-mail: lmpeng@pku.edu.cn.
[†] Chinese Academy of Science.
[‡] Peking University.

10.1021/jp061599d CCC: $33.50 
Published on Web 06/16/2006

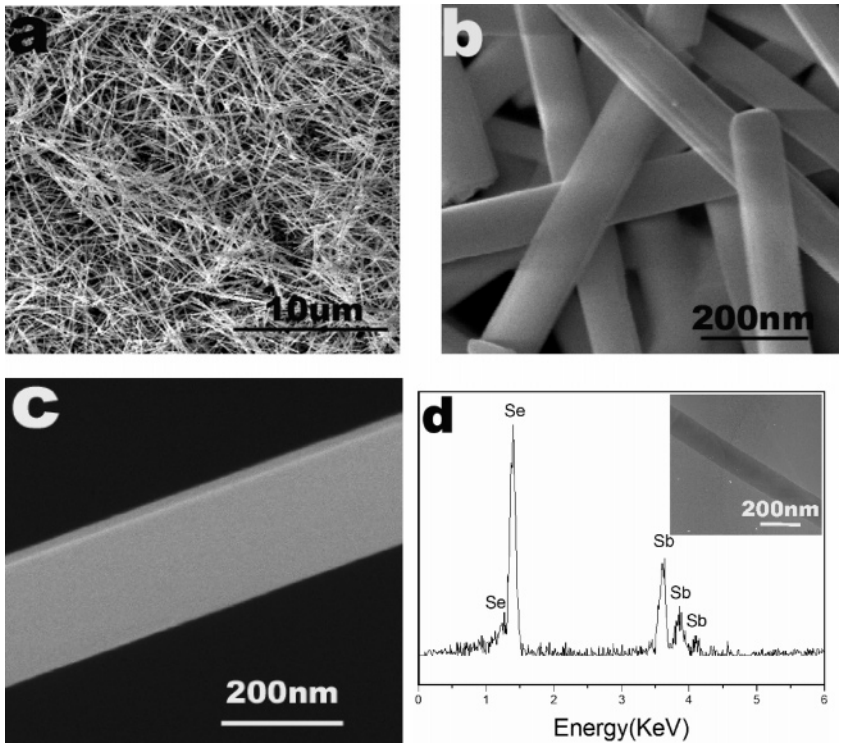


**Figure 1.** Morphology and composition analysis of $Sb_2Se_3$ nanoribbons. (a) Low magnification SEM image of the products showing that the product contains a large quantity of wirelike 1D materials. (b) High magnification SEM image of the products revealing that the 1D material has a nanoribbon structure. (c) SEM image showing a single nanoribbon with rectangular cross sections. The thickness of the ribbon is estimated to be about 50 nm, and the width is estimated to be about 185 nm. (d) EDX spectrum taken from a single nanoribbon giving the nanoribbons a possible composition of $Sb_2Se_3$. The insert TEM image in (d) shows a typical $Sb_2Se_3$ nanoribbon used in EDX experiment.

washed with distilled water to remove ions remaining in the products. The final products were then dried in air. $Sb_2S_3$ nanoribbons was obtained by using 0.1 g of sulfur powder replacing 0.2 g of selenium powder, and the necessary reaction time was about 12 h, with no other changes needed.

Powder X-ray diffraction (XRD) experiments were performed with a Rigaku D/max 2400 diffractometer using monochromatic Cu K$\alpha$ radiation ($\lambda = 1.54$ Å), 40 kV and 120 mA, and scanning between 5° and 65° ($2\theta$). Transmission electron microscopy (TEM) studies were performed using a Philips Tecnai 20 high-resolution transmission electron microscope and a Philips CM200/FEG field-emission-gun transmission electron microscope, both operated at 200 kV. Scanning electron microscopy (SEM) observations were carried out using a XL30 S-FEG (FEI SIRION) field-emission scanning electron microscope. The composition of the specimens was analyzed using energy-dispersive X-ray spectroscopy (EDX) attached to the Tecnai 20. The specimens for TEM studies were prepared by dispersing the products in alcohol followed by ultrasonic treatment. The sample was then dropped onto a holey carbon film supported on a copper grid and dried in air. The band gap energy of the product was determined from the onset of the absorbance spectra of the sample on a UV−vis−NIR spectrophotometer (Shimadzu UV-3100).

### 3. Results and Discussion

The morphologies of $Sb_2Se_3$ nanoribbons were examined with a field-emission scanning electron microscope. Three SEM images of the product taken at different magnifications are shown in Figure 1a−c. Figure 1a shows that the product contains a large quantity of wirelike materials without any visible byproducts, suggesting that the product is of high quality. The lengths of the products range from tens of microns to hundreds of microns. Figure 1b shows a higher magnification SEM image revealing that the width of the one-dimensional (1D) material is much larger than its thickness, and closer inspection shows that the products have rectangular cross sections; that is, the geometric shape of the 1D product appears to be that of a nanoribbon structure. Figure 1c shows a single nanoribbon with a cross section of about 185 nm in width and 50 nm in thickness. Extensive TEM and SEM observations reveal that the nanoribbons are typically 100−300 nm in width and 20−60 nm in thickness. To determine the composition of the nanoribbons, EDX experiments were performed on individual nanoribbons. Figure 1d is an EDX spectrum obtained from a single nanoribbon (about 140 nm in width) as shown in the insert of Figure 1d. Only Sb and Se peaks are observed in this spectrum, suggesting that the nanoribbon is composed of mainly Sb and Se. Quantitative EDX analysis shows that the atom ratio of Sb:Se is 40.3:59.7, close to 2:3, giving the nanoribbons a possible composition of $Sb_2Se_3$.

X-ray powder diffraction (XRD) analysis was used to determine the structure of the $Sb_2Se_3$ nanoribbons. The results are shown in Figure 2. All the peaks in Figure 2 may be well indexed using the orthorhombic phase of $Sb_2Se_3$ (cell constants $a = 11.63$ Å, $b = 11.78$ Å, $c = 3.985$ Å; JCPDS 15-0861). No peaks of any other phases were detected, indicating that our nanoribbon sample is a very high purity single-phase sample.

The structure of the $Sb_2Se_3$ nanoribbons is further investigated using high-resolution transmission electron microscopy (HRTEM) and electron diffraction (ED). An HRTEM image of a single $Sb_2Se_3$ nanoribbons is shown in Figure 3, where the insert is the corresponding ED pattern. Like the XRD profile of Figure 2, both the HRTEM image and the ED pattern can be indexed using the orthorhombic phase of $Sb_2Se_3$ (JCPDS 15-0861). A further confirmation of the $Sb_2Se_3$ nanoribbon structure is

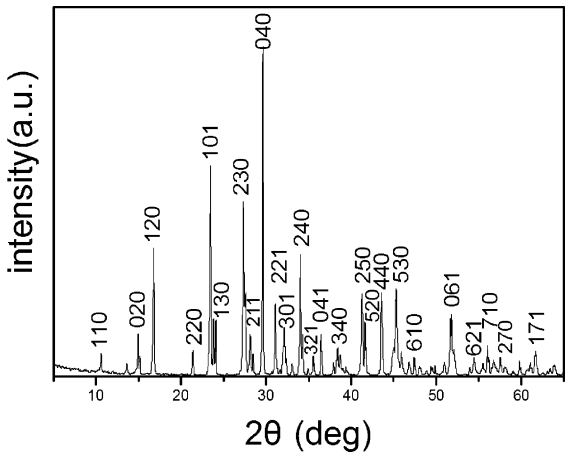


**Figure 2.** XRD profile recorded from the nanoribbon sample. It is well indexed using the orthorhombic phase $Sb_2Se_3$ (JCPDS 15-0861).

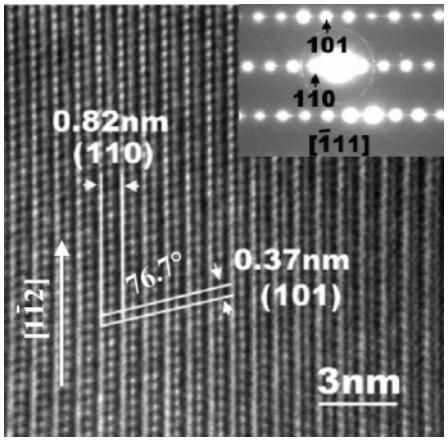


**Figure 3.** HRTEM image showing a $Sb2Se_3$ nanoribbon. The insert is the corresponding ED pattern taken along the [$\bar{1}$11] zone axis.

obtained. In Figure 3 the lattice spacings of 0.82 and 0.37 nm correspond to the (110) and (101) plane spacings of orthorhombic phase $Sb_2Se_3$, respectively. The angle between the ($\bar{1}$10) and (101) planes is 76.7°. The ED pattern taken along the [$\bar{1}$11] zone axis is a spot pattern, revealing that the nanoribbon is single crystal in nature. Both the HRTEM image and ED pattern demonstrate that the nanoribbon grows along the [1$\bar{1}$2] direction indicated with an arrow in Figure 3, and this growth direction is different from what was reported previously for $Sb_2Se_3$ nanoribbons.[30] Figure 3 also reveals that the nanoribbon quality is very high, free from dislocation and stacking faults.

To understand the growth mechanism of $Sb_2Se_3$ nanoribbons, extensive TEM observations were performed on samples synthesized with different hydrothermal reaction times, and the results are shown in Figure 4. In a typical experiment, $SbCl_3$ was strongly hydrolyzed in water, producing white precipitates of SbOCl. Once Se and $NaBH_4$ were introduced, $NaBH_4$ first reacted with water to produce $H_2$; $H_2$ then reacted with Se to produce $H_2Se$. During our experiment, we can smell the odor of gas, which verifies the existence of $H_2Se$. $H_2Se$ then reacts with SbOCl to produce $Sb_2Se_3$. Because $Sb_2Se_3$ has a far smaller solubility than that of SbOCl, SbOCl is unstable in the hydrothermal condition and the reaction may therefore proceed spontaneously.

Figure 4a is a low magnification TEM image of the sample after hydrothermal reaction for 1 h, showing that the sample consists of granular crystals in size ranging from 3 to 8 nm. Figure 4b is an HRTEM image of the same sample, where the insert is the corresponding ED pattern taken from an area containing many nanoparticles. Both the lattice spacing and the ED pattern can be indexed using the orthorhombic phase of $Sb_2Se_3$ (JCPDS 15-0861), verifying that nanoparticles are indeed $Sb_2Se_3$ particles. After hydrothermal reaction for 3 h, many short nanoribbons formed ranging from several hundred nanometers

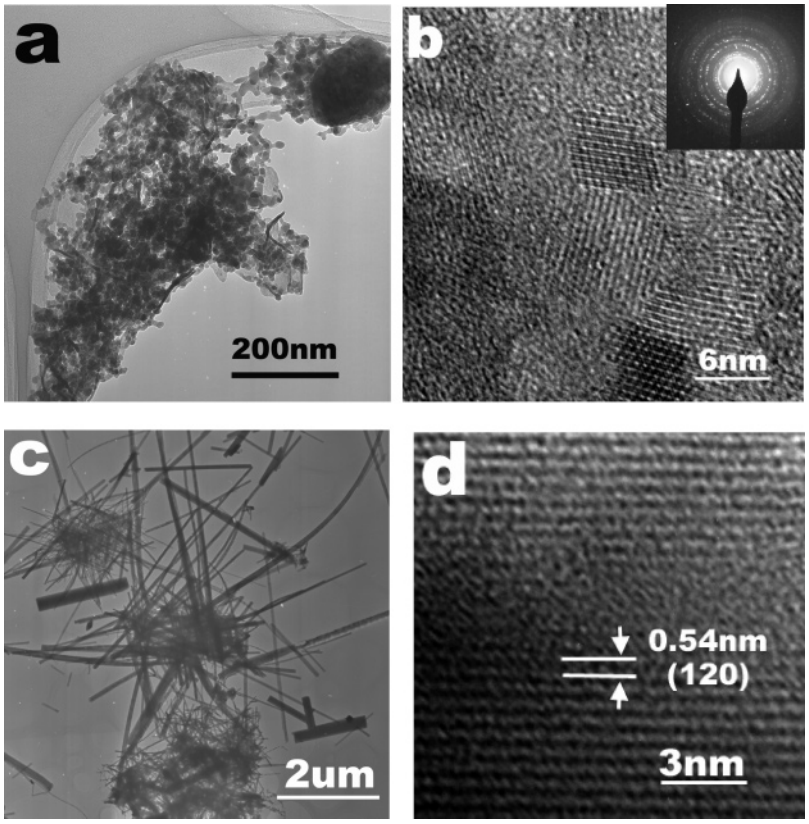


**Figure 4.** Series of TEM and HRTEM images showing the growth process of $Sb_2Se_3$ nanoribbons. (a) and (b) show some $Sb_2Se_3$ granular crystals after hydrothermal reaction for 1 h. (c) and (d) show that nanoribbons began to appear after reaction for 3 h.

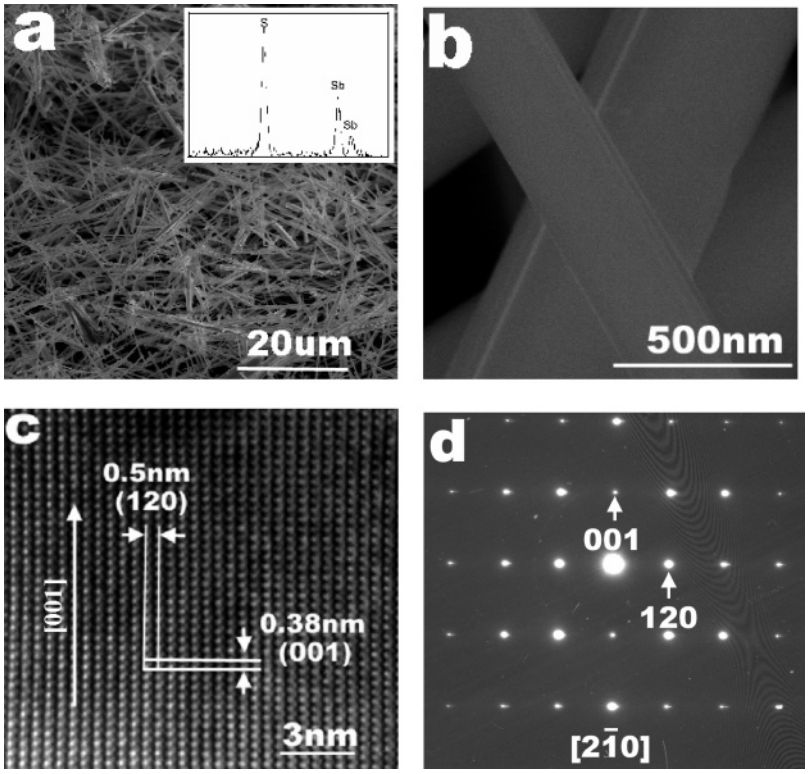


**Figure 5.** Morphology, composition, and structure analysis of $Sb_2S_3$ nanoribbons. (a) Low magnification SEM image of the product showing that the product contains a large quantity of 1D materials. The insert is the corresponding EDX spectrum giving the 1D sample a possible composition of $Sb_2S_3$. (b) High magnification SEM image of the products revealing that the 1D materials are indeed have nanoribbon structure. (c) and (d) are HRTEM image and corresponding ED pattern, respectively. Both HRTEM image and SAED pattern were indexed as the orthorhombic phase of $Sb_2S_3$ (JCPDS 42-1393).

to several microns in length as shown in Figure 4c. The higher magnification TEM image shown in Figure 4d reveals that the structure of the short nanoribbons is the same as that of $Sb_2Se_3$. We concluded therefore that the nanoribbons grew from merging $Sb_2Se_3$ particles of Figure 4a,b. Figure 4d shows that the quality of these short nanoribbons is rather poor. They are highly disordered and not fully crystallized. Longer reaction times subsequently reduced the disordered and amorphous phase, giving much better quality and longer nanoribbons. To understand the role of glycol solution on the growth of $Sb_2Se_3$ nanoribbons, glycol solution was replaced by deionized water. It was found that the sample after reaction for 1 h consisted also of granular crystals of $Sb_2Se_3$ but having much larger diameters of about 80−120 nm. After hydrothermal treatment for 3 days, the final products contained mainly larger particles and nanorbbons in modicum, suggesting that glycol solution might act effectively as a kind of stabilizer, to prevent the $Sb_2Se_3$ particles from aggregating into larger ones; i.e., it controlled the size of the $Sb_2Se_3$ particles. On the basis of our experiments, we propose the following four relevant chemical reactions for the growth process of $Sb_2Se_3$ nanoribbons:

$$SbCl_3 + H_2O \leftrightarrow SbOCl + 2HCl \quad \text{(a)}$$

$$NaBH_4 + 2H_2O + 4Se \leftrightarrow Na^+ + BO_2^- + 4Se^{2-} + 8H^+ \quad \text{(b)}$$

$$2SbOCl + 3Se_2^- + 2H_2O \leftrightarrow Sb_2Se_3 + 4OH^- + 2Cl^- \quad \text{(c)}$$

$$nSb_2Se_3 \leftrightarrow Sb_2Se_{3\text{nanoribbons}} \quad \text{(d)}$$

$Sb_2S_3$ nanoribbons were obtained by using 0.1 g of sulfur powder replacing 0.2 g of selenium powder, and shortening the reaction time to 12 h, without any other changes needed. Figure 5a shows a low magnification SEM image of the products, showing that the product contains a large quantity of wirelike materials. The lengths of the products range from tens of microns to hundreds of microns. The insert in Figure 5a is an EDX spectrum taken from an area consisting of many samples. Only Sb and S peaks are observed in this spectrum, suggesting that the 1D sample is composed of mainly Sb and S. Quantitative EDX analysis shows that the atom ratio of Sb:Se is 37:63, close to 2:3, giving the sample a possible composition of $Sb_2S_3$. Closer inspection revealed that the geometric shape of the 1D sample appears to be that of a nanoribbon structure. Figure 5b clearly displays the side surfaces of two nanoribbons having rectangular cross sections. One is about 190 nm in width and 30 nm in thickness, and the other one is about 450 nm in width and 80 nm in thickness. Extensive TEM and SEM observations reveal that the nanoribbons are typically 200−500 nm in width and 20−80 nm in thickness.

The structure of $Sb_2S_3$ nanoribbons was characterized using XRD, HRTEM, and selected area electron diffraction (SAED). The XRD profile (not given in this paper) shows that the nanoribbon structure is of the orthorhombic phase of $Sb_2S_3$ (cell constants $a = 11.23$ Å, $b = 11.31$ Å, $c = 3.841$ Å; JCPDS 42-1393), which is identical to that reported in our previous work for $Sb_2S_3$ nanoribbons.[31] Figure 5c,d shows a HRTEM image of a single $Sb_2S_3$ nanoribbon and its corresponding ED pattern. Like the XRD profile, the HRTEM image and the ED pattern may also be indexed using the orthorhombic phase of $Sb_2S_3$ (JCPDS 42-1393). The lattice spacings of 0.5 and 0.38 nm marked in Figure 5c correspond respectively to the (120) and (001) plane spacing of orthorhombic phase $Sb_2S_3$. The angle between the (120) and (001) planes is 90°. The ED pattern taken along the [2$\bar{1}$0] zone axis is a spot pattern, suggesting that the nanoribbons are single

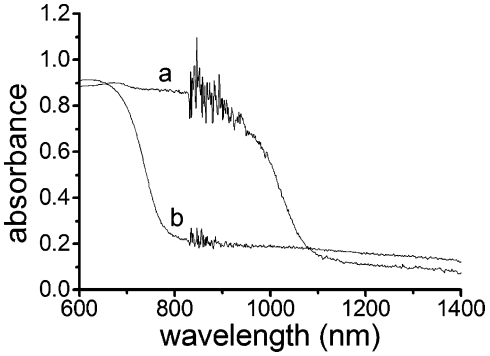


**Figure 6.** Experimental UV−visible spectrum taken from (a) $Sb_2Se_3$ nanoribbons and (b) $Sb_2S_3$ nanoribbons.

crystalline in nature. Both the HRTEM image and ED pattern demonstrate that the nanoribbon grows along the [001] direction indicated with an arrow in Figure 5c, which coincides with that previously reported for $Sb_2S_3$ nanoribbons.[31] Like $Sb_2Se_3$ nanoribbons growing from $Sb_2Se_3$ particles, $Sb_2S_3$ nanoribbons also grew from $Sb_2S_3$ particles. This is different from the previous report that the $Sb_2S_3$ nanoribbons grew from the decomposition of one kind of amorphous compound of $Sb_xS_yO_z$.[31] The role of glycol solution in the growth of $Sb_2S_3$ nanoribbons is less important than in that of $Sb_2Se_3$ nanoribbons. Without glycol solution, we can obtain more and better quality $Sb_2S_3$ nanoribbons than $Sb_2Se_3$ nanoribbons in the same condition, which might result from the different reaction speed between $Sb_2S_3$ and $Sb_2Se_3$ nanoribbons.

An optical absorption experiment was carried out to elucidate information on the band gap energy, which is one of the most important electronic parameters for semiconductor nanomaterials. Figure 6 shows two typical UV−visible absorption spectra taken from $Sb_2Se_3$ and $Sb_2S_3$ nanoribbons. Since all experimental results, including XRD, ED, EDX, TEM, and SEM observations, suggest that both $Sb_2Se_3$ and $Sb_2S_3$ nanoribbons are in pure high-quality crystalline phases, we suppose that the absorption spectrum represents the true absorption behavior of $Sb_2Se_3$ and $Sb_2S_3$ nanoribbons. Curve a in Figure 6 is the absorption spectrum recorded from $Sb_2Se_3$ nanoribbons showing that the $\lambda_{onset}$ of the spectrum is about 1080 nm. Curve b in Figure 6 shows the absorption spectrum recorded from $Sb_2S_3$ nanoribbons giving the $\lambda_{onset}$ of the spectrum at about 780 nm. The band gap of $Sb_2Se_3$ nanoribbons and $Sb_2S_3$ nanoribbons may be estimated at 1.15 and 1.56 eV, respectively, using the following formula:

$$\alpha = \sqrt{h\nu - E_g}/h\nu$$

where $h\nu$ is the corresponding phonon energy, and $\alpha$ is the absorbance coefficient. The experimental values of the band gap for $Sb_2Se_3$ and $Sb_2S_3$ nanoribbons are near the optimum value for photovoltaic conversion, suggesting that $Sb_2Se_3$ and $Sb_2S_3$ nanoribbons may be very promising for applications in solar energy and photoelectronics.

## 4. Conclusion

Large-scale ultralong single-crystalline $Sb_2Se_3$ and $Sb_2S_3$ nanoribbons were prepared by reacting $SbCl_3$ with selenium and sulfur powders in glycol solution. Both $Sb_2Se_3$ and the $Sb_2S_3$ nanoribbons are hundreds of microns in length, and the structure of the nanoribbons is determined to be of the orthorhombic phase. $Sb_2Se_3$ nanoribbons are typically 100−300 nm in width and 20−60 nm in thickness and grow along the $[1\bar{1}2]$ direction. $Sb_2S_3$ nanoribbons are wider than $Sb_2Se_3$ nanoribbons, about 200−500 nm in width, and grow along the [001] direction. The growth mechanism of the nanoribbons was investigated based on HRTEM observations. It was found that glycol solution may act effectively as a kind of stabilizer, preventing $Sb_2Se_3$ and $Sb_2S_3$ particles from aggregating into larger ones, and this is crucial for the growth of high-quality crystalline nanoribbnons. An optical absorption experiment reveals that $Sb_2Se_3$ and $Sb_2S_3$ nanoribbons are two semiconductors with bandwidth $E_g \approx 1.15$ and 1.56 eV, respectively.

**Acknowledgment.** The authors are grateful for the support of the Ministry of Science and Technology (Grant 001CB610502), the National Science Foundation of China (Grant 10434010), the Chinese Ministry of Education (Key Project Grant No. 10401), and the National Center for Nanoscience and Technology of China.

## References and Notes

(1) Huang, Y.; Duan, X. F.; Cui, Y.; Lauhon, L. J.; Kim, K. H.; Lieber, C. M. *Science* **2001**, *294*, 1313.
(2) Bachtold, A.; Hadley, P.; Nakanishi, T.; Dekker, C. *Science* **2001**, *294*, 1317.
(3) Yu, Y.; Jin, C. H.; Wang, R. H.; Chen, Q.; Peng, L.-M. *J. Phys. Chem. B* **2005**, *109*, 18772.
(4) Goriunova, N. A.; Kolomiets, B. T.; Mal'kova, A. A. *Sov. Phys. Tech. Phys.* **1956**, *1*, 1583.
(5) Arivouli, D.; Gnanam, F. D.; Ramasamy, P. *J. Mater. Sci. Lett.* **1988**, *7*, 711.
(6) Case, T. W. *Phys. Rev.* **1917**, *9*, 305.
(7) Hofmann, W. *Z. Kristallogr.* **1933**, *86*, 225.
(8) Scavnicar, S. *Z. Kristallogr.* **1960**, *114*, 49.
(9) Rosi, F. D.; Abeles, B.; Jensen, R. V. *J. Phys. Chem. Solids* **1959**, *10*, 191.
(10) Platakis, N. S.; Gatos, H. C. *Phys. Status Solidi A* **1972**, *13*, K1.
(11) Rajapure, K.; Lokhande, C.; Bhosele, C. *Thin Solid Films* **1997**, *311*, 114.
(12) Kim, I. *Mater. Lett.* **2000**, *43*, 221.
(13) Roy, B.; Chakbraborty, B. R.; Bhattacharya, R.; Dutta, A. K. *Solid State Commun.* **1978**, *25*, 937.
(14) Savadogo, O.; Mandal, K. C. *Sol. Energy Mater. Sol. Cells* **1992**, *26*, 117.
(15) Abrikosov, N. Kh.; Bankina, V. F.; Poretakaya, L. V.; Skudnova, L. E.; Skudnova, E. V. In *Semiconducting II-VI and V-VI Compounds*; Tybulewicz, A., Ed.; Plenum: New York, 1969; p 186.
(16) Pramanik, P.; Bhattacharya, R. N. *J. Solid State Chem.* **1982**, *44*, 425.
(17) Fernandez, A. M.; Merino, M. G. *Thin Solid Films* **2000**, *366*, 202.
(18) Arun, P.; Vedeshwar, A. G. *J. Appl. Phys.* **1996**, *79*, 4029.
(19) Lokhande, C. D. *Chem. Phys.* **1991**, *27*, 1.
(20) Wang, J. W.; Deng, Z. X.; Li, Y. D. *Mater. Res. Bull.* **2002**, *37*, 495.
(21) Yang, J.; Zeng, J. H.; Yu, S. H.; Yang, L.; Zhang, Y. H.; Qian, Y. T. *Chem. Mater.* **2000**, *12*, 2924.
(22) Wang, J. W.; Li, Y. D. *Mater. Chem. Phys.* **2004**, *87*, 420.
(23) Jiang, Y.; Zhu, Y. J. *J. Phys. Chem. B* **2005**, *109*, 4361.
(24) Zheng, X. W.; Xie, Y.; Zhu, L. Y.; Jiang, X. C.; Jia, Y. B.; Song, W. H.; Sun, Y. P. *Inorg. Chem.* **2002**, *41*, 455.
(25) Yang, J.; Liu, Y. C.; Lin, H. M.; Chen, C. C. *Adv. Mater.* **2004**, *16*, 713.
(26) Pan, Z. W.; Dai, Z. R.; Wang, Z. L. *Science* **2001**, *291*, 1947.
(27) Wang, Z. L.; Pan, Z. W. *Adv. Mater.* **2002**, *14*, 1029.
(28) Comini, E.; Faglia, G.; Sberveglieri, G.; Pan, Z. W.; Wang, Z. L. *Appl. Phys. Lett.* **2002**, *81*, 1869.
(29) Liu, Z. P.; Peng, S.; Xie, Q.; Hu, Z. K.; Yang, Y.; Zhang, S. Y.; Qian, Y. T. *Adv. Mater.* **2003**, *15*, 936.
(30) Xie, Q.; Liu, Z. P.; Shao, M. W.; Kong, L. F.; Yu, W. C.; Qian, Y. T. *J. Cryst. Growth* **2003**, *252*, 570.
(31) Yu, Y.; Wang, R. H.; Chen, Q.; Peng, L.-M. *J. Phys. Chem. B* **2005**, *109*, 23312.